Hindawi
Advances in Condensed Matter Physics
Volume 2020, Article ID 9635917, 8 pages
https://doi.org/10.1155/2020/9635917

Research Article

Electronic Structure and Room Temperature of 2D Dilute Magnetic Semiconductors in Bilayer MoS_2-Doped Mn

Sintayehu Mekonnen Hailemariam

Department of Physics, College of Natural Sciences, Arbaminch University, Arbaminch, Ethiopia

Correspondence should be addressed to Sintayehu Mekonnen Hailemariam; hailemariamsintayeh@gmail.com

Received 16 October 2019; Accepted 23 November 2019; Published 20 January 2020

Academic Editor: Ward Beyermann

The electronic structure and magnetic properties of manganese- (Mn-) doped bilayer (BL) molybdenum disulfide (MoS_2) are studied using the density function theory (DFT) plus on-site Hubbard potential correction (U). The results show that the substitution of Mn at the Mo sites of BL MoS_2 is energetically favorable under sulfur- (S-) rich regime than Mo. The magnetic interaction between the two manganese (Mn) atoms in BL MoS_2 is always ferromagnetic (FM) irrespective of the spatial distance between them, but the strength of ferromagnetic interaction decays with atomic distance. It is also found that two dopants in different layers of BL MoS_2 communicate ferromagnetically. In addition to this, the detail investigation of BL MoS_2 and its counterpart of monolayer indicates that interlayer interaction in BL MoS_2 affects the magnetic interaction in Mn-doped BL MoS_2. The calculated Curie temperature is 324, 418, and 381 K for impurity concentration of 4%, 6.25%, and 11.11%, respectively, which is greater than room temperature, and the good dilute limit of dopant concentration is 0–6.25%. Based on the finding, it is proposed that Mn-doped BL MoS_2 are promising candidates for two-dimensional (2D) dilute magnetic semiconductor (DMS) for high-temperature spintronics applications.

1. Introduction

It is known that graphene is the most well-known member in the family of 2D materials. However, its gapless band structure has been deemed as a considerable drawback for realizing switching operation which is essential for digital logic devices [1]. On contrary to zero band gap graphene, other group of 2D materials so called transition metal dichalcogenides (TMDS) with chemical formula MX_2, where M stands for transition metals like molibidium (Mo), tungeston (W), and so on and X stands for chalcogen atoms like selfur (S), selenium (Se), and telenium (Te), and so on are more recently discovered [2]. The experimental study reveals that the weak van der Waals forces between each 2D monolayer of which they are formed allow thin multilayers to be easily exfoliated from their bulk form [3]. Among those families, monolayer MoS_2 and few layer MoS_2 have attracted interest due to their potential application [2, 4]; for instance, the monolayer (ML) MoS_2 has emerged as a semiconductor with a large intrinsic direct band gap of approximately 1.8 eV [3], which makes it suitable for nanoelectronic and optoelectronic applications [5]. In MoS_2 materials, the electronic structure depends on the number of layers which mean that there is a gradual transition from an indirect band gap (1.3 eV) in the bulk material to a direct gap in the ML material with band gap 1.9 eV which reveals that the interlayer van der Waals (VdW) interaction may affect the electronic structure [6]. In addition, it has been reported that the electronic structure of such system depends on stacking patterns [7]. There are five different stacking configurations for the bilayer MoS_2 system [7], but the most stable one is AA' [8].

On the contrary, during last few decades, the research in dilute magnetic semiconductors (DMSs) have attracted tremendous interest due to their great potential for different spin electronics (spintronics) applications [9]. Spintronics refers to new phenomena of electronic transport for which the electron spin plays a decisive role in contrast to

conventional electronics for which the electron spin is practically irrelevant. For a full exploitation of spintronics, one should have materials which show simultaneously semiconducting properties and ferromagnetic ordering at operational temperature [10]. In last two decades, most of DMS research has focused on the transition metal- (TM-) doped III-V and II-VI three-dimensional (3D) semiconductors. However, the ferromagnetic transition temperature in well-studied type of DMSs like Ga_{1-x} Mn_x As is less than 200 K which is far from room temperature [11]. As a result of this, the search for DMS has recently been extended to two-dimensional (2D) transition metal dichalcogenides (TMDs) like MoS_2-, $MoSe_2$-, and WS_2-doped transition metal [4]. Recent theoretical study reveals that Mn and Fe are the best candidates to generate long-range room temperature in its Ml phase [4]. To date, several groups have reported experimentally [12] and theoretically the feasibility of MoS_2 by substitutional doping with different (TM) : Mn-doped monolayer (ML) MoS_2 [13], iron- (Fe-) doped bilayer MoS_2 [14], Ni-doped ML MoS_2 [15], and Co-doped monolayer MoS_2 [16]. In addition to this, in our previous ab initio study, we have shown that V-doped ML and BL MoS_2 are good candidates for nearly room temperature ferromagnetism [17]. However, electronic structure and magnetic interaction in Mn-doped bilayer (BL) MoS_2 has not yet been studied in detail. In this current study, Mn-doped BL MoS_2 are studied on the basis of spin polarized (DFT + U) formalism. The relative structural stability, electronic structure, and magnetic properties of MoS_2-doped Mn are studied in detail. To understand magnetic ground state and the magnetic energy ΔE, the energy difference between two dopants in FM and AF cofigurations in the ML and BL phase of MoS_2 was calculated for different impurity concentrations. Furthermore, based on mean field theory together with empirical correction, the Curie temperature (Tc) is also estimated.

2. Computational Details

DFT + U calculations were performed using the plane-wave pseudopotential method with the aid of QUANTUM ESPRESSO code. On-site Hubbard parameter, $U = 4$ eV, was assigned for dopants to take into account the strong correlation in the Mn 3d state [18]. Ultrasoft pseudopotentials (UPPs) were used to deal with the interaction between valence electrons and the ion core. The plane wave basis set is given a cutoff energy of 60 Ry used after performing the convergence test with respect to total energy. A unit cell with the periodic boundary condition was adopted to simulate the infinite x-y plane. For the BL crystal, Grimmes DFT-D2 dispersion correction [19] was applied to account for the long-range van der Waals interactions between layers. The equilibrium interlayer distance was obtained by careful minimization of total energy with respect to distance between layers. To investigate the doping effects of Mn impurities on bilayer MoS_2, the BL MoS_2 was modeled by supercell of $(3 \times 3 \times 1)$, $(4 \times 4 \times 1)$, and $(5 \times 5 \times 1)$ which contains 36 S and 18 Mo, 64 S and 32 Mo, and 50 Mo and 100 S atoms, respectively. The vacuum space 20 Å thickness along the z axis was used to avoid any self-interaction of the slabs for ML (to make sure there is no interaction along the z-axis). Integrations over the Brillouin zone (BZ) were sampled based on a Monkhorst pack 2D grid [20] based on the size of supercells.

3. Result and Discussion

3.1. Defect Formation Energy and Structural Stability. To understand relative stability of dopant atom (Mn) in BL MoS_2, dopant formation energy (E_{form}) was carried out employing the following equation [17, 21]:

$$E_{\text{form}} = E(\text{Mn}, \text{MoS}_2) - E(\text{MoS}_2) - \sum_i n_i (\mu_{\text{Mn}} - \mu_{\text{Mo}}), \quad (1)$$

where E (Mn, MoS_2) and E (MoS_2) are total energy of doped and pure BL MoS_2, respectively, n_i is the corresponding number of species that has been added to or removed from the supercell, and μ_{Mn} and μ_{Mo} are chemical potentials of Mn and Mo, respectively. Both Mo- and S-rich conditions were considered for chemical potential calculation of Mo. In the Mo-rich condition, the chemical potential for μ_{Mo} is obtained from its bulk body-centered cubic (BCC) structure of Mo [21], whereas, under the S-rich condition, μ_{Mo} is obtained from energy difference between formula unit of MoS_2 and ring form of sulfur molecules. The dopant formation energy calculated using equation (1) for different impurity configurations of impurity atoms is summarized in Table 1. All calculated values under the S-rich condition is negative which reveal that doping Mn under the S-rich condition of BL MoS_2 is favorable in comparison with the Mo-rich condition in agreement with previous theoretical report [21] and experimental result [22]. Besides to this, the least formation energy −2.0144 eV is obtained in doping single Mn on $4 \times 4 \times 1$ BL MoS_2 (6.25%) compared to $3 \times 3 \times 1$ (11.11% Mn doping) which indicates that Mn dopants are more energetically favorable to occupy the substitutional lattice site (Mo) at low impurity concentration (dilute magnetic limit) than at high concentration.

3.2. Electronic Structures and Magnetism of Pure and Single Mn-Doped BL MoS_2. The calculated equilibrium lattice constant after optimization is 3.18 Å, which is closer to the experimental value [23] and in good agreement with theoretical value 3.18 Å [24]. In addition to this, the calculated interlayer distance (the distance between two ML) of BL MoS_2 is found to be 6.543 Å and the band gap calculated at this interlayer distance is 1.3 eV (Figure 1) closer with the previous reported value 1.29 Å [25]. Furthermore, the band gap increases with increasing interlayer distance, as shown in Figure 1(a). To investigate the effects of single Mn doping on the electronic and magnetic properties of pure BL MoS_2, $4 \times 4 \times 1$ and $3 \times 3 \times 1$ BL MoS_2 model supercells which result in a magnetic impurity concentration of 3.125% and 5.55%, respectively, after doping a single Mn atom were considered (see Figure 2). As seen from Table 2, the total magnetic moment of the system is 1 and 1.02 μ_B after

Table 1: The calculated values of formation energy (E_{form} (eV)) under Mo-rich and S-rich growth conditions.

Supercell	Doping site	Mo rich (E_{form} (eV))	S rich (E_{form} (eV))
$3 \times 3 \times 1$	1 Mn	1.908	−0.7523
>>	N	3.4019	−1.9173
>>	NN	3.7658	−1.5534
>>	NNN	3.4027	−1.9184
>>	Updn(do)	3.9779	−1.3432
>>	Updn(d1)	3.9806	−1.3406
$4 \times 4 \times 1$	1 Mn	1.8677	−0.7919
>>	N	3.3067	−2.0144
>>	NN	3.6618	−1.6580
>>	NN N	3.70856	−1.6126
>>	Updn(do)	3.7319	−1.5873
>>	Updn(d1)	3.7381	−1.5811

introducing single Mn in supercell of $3 \times 3 \times 1$ and $4 \times 4 \times 1$, respectively.

To understand how the states are distributed, the total density of state (DOS) for pure and single Mn-doped BL MoS_2 is plotted. As shown from Figure 3(a), for the pure system, the Fermi level is located at the middle and spin up and spin down states are symmetric indicating the pure BL MoS_2 are nonmagnetic semiconductors. However, after introducing single Mn, the spin degeneracy of the band structure is broken and the minority of states remain semiconductors, whereas the majority (spin up state) impurity state is formed in the vicinity of the Fermi level; as a result, it behaves as metallic, leading to magnetic and half metallic behavior of the total DOS. On the contrary, with increasing concentration of Mn dopant (3.125% to 11.11%), the impurity state is broaden (moves closer to conduction band minimum (CBM)) Figures 3(b)–3(e) which reveals that the doped system behaves as the n-type of semiconductor. Furthermore, to understand the nature of band structure and defect state, the band structure of pure and single Mn doped in one of its layers is plotted. As shown from Figures 4(a) and 4(b), the pure system is nonmagnetic semiconductor with direct band gap measured to be 1.3 eV. However, in single Mn-doped system, the majority band structure and the impurity states are formed above the Fermi level (within the gap) (Figure 4(c)). But, the minority state remains semiconductor, but the band gap is suppressed by 0.1 eV compared to the pure system (Figure 4(d)), which also gives further confirmation half metallic and magnetic behavior of the doped system. On the contrary, the impurity state closer to CBM reveals that the system is more likely the n-type of semiconductor. Based on those observation, it is suggested that the origin of magnetism as an isolated Mn atom with electron configuration $[Ar]3d^5 4S^2$ has one more d-orbital electron than Mo (with electron configuration $[Ar]3d^4 4S^2$); thus, the extra one electron is responsible for the observed defect state in the gap.

3.3. Magnetic Interaction between Dopants in Monolayer (ML) and Bilayer (BL) MoS_2 Doped with a Pair of Mn Atoms. The magnetic interaction between dopants in doped ML and BL MoS_2 systems is studied by calculating the total energy difference between FM and AF configurations at the same impurity separation [17]. The magnetic energy (ΔE) is given by

$$\Delta E = E_{\text{FM}} - E_{\text{AF}}, \tag{2}$$

where E_{FM} and E_{AF} are the total energies of the supercell in FM and AF states, respectively. Employing model supercells, $5 \times 5 \times 1$, $4 \times 4 \times 1$, and $3 \times 3 \times 1$ MoS_2 result in doping concentrations 4%, 6.25%, and 11.11%, respectively. Five configurations with different dopant-dopant (Mn-Mn) separations were considered: nearest-neighbor (N) configuration in which the two Mn atoms are in the nearest neighboring position with Mn-Mn distance of 3.4 Å, the second nearest-neighbor (NN) configurations in which the two Mn atoms are in the next nearest-neighboring position with Mn-Mn distance of 5.5 Å, and the third nearest-neighbor (NNN) configuration in which the distance between the two doped Mn atoms are 6.4 Å; two Mn atoms in different layers of BL MoS_2 are separated by interlayer distance (updn(d_0) = 6.53 Å), and two Mn atoms in different layers of BL MoS_2 are separated by interlayer distance (updn(d_1) = 7.8 Å) results summarized in Tables 2 and 3. As can be seen from Tables 2 and 3, the calculated ΔE for all impurity configurations are negative which show that FM interaction is favorable for all concentrations of impurity in agreement with previous study in ML MoS_2-doped Mn [26]. In addition to that, the strength of FM interaction decays from N to NNN for all concentrations of impurity. Furthermore, in order to get insights into FM interaction between the two nearest neighbor (N) Mn dopants, the total density of states (DOS) are plotted as shown in Figures 3(e) and 3(e); the dopants are ferromagnetically interacting, and the impurity states push towards the CBM with increasing impurity concentration (6.25–11.11%), which is in broad agreement with dilute magnetic semiconductor properties [11]. We further extend our investigation by doping two Mn in different layers BL MoS_2, as seen in the input structure in Figure 2(d) and Table 4, and $\Delta E = -0.006$ and -0.0025 eV when two dopants are separated by $d_0 = 6.53$ Å (at equilibrium interlayer distance) and $d = 7.8$ Å, respectively. Interestingly, the result reveals that two dopants in different layers can interact ferromagnetically, and the strength of ferromagnetism suppresses with atomic distance and impurity concentration. This is also seen in the DOS plot in Figure 3(e), where spin degeneracy of spin up and spin down is breaking and system becomes ferromagnetic. For further information, the electronic band structure is drawn, as shown from the band plot for those system seen in Figures 4(e) and 4(f), the system becomes magnetic even when two dopants are in different layers, and this makes the physics of system under investigation more interesting that how two dopants in different layers are communicating. On the contrary, understanding mechanism of exchange interaction in magnetic system is another issue. Goodenough–Kanamori–Anderson rules which state that the magnetic ion-ligand-magnetic ion angle is 180° of two magnetic ions with partially filled d shells is strongly antiferromagnetic, whereas the magnetic ion-ligand-magnetic ion angle is 90° and is ferromagnetic super exchange. Thus,

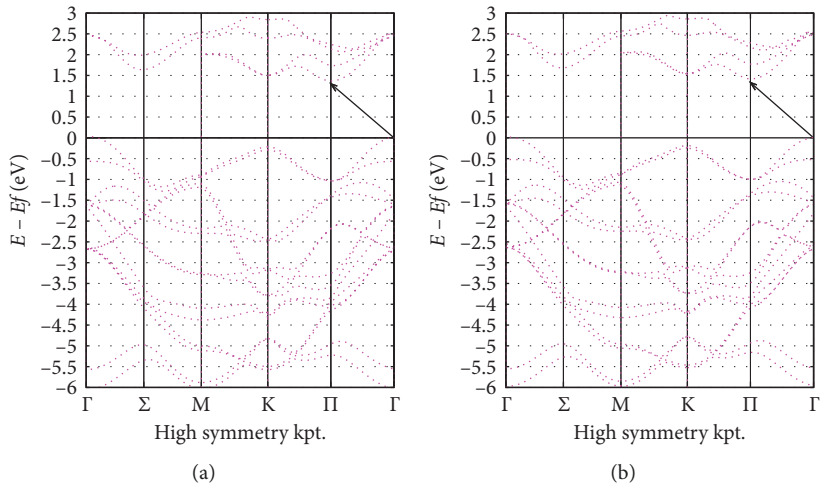

Figure 1: The calculated interlayer distance-dependent band structure of BL MoS_2: the band structure calculated at (a) equilibrium interlayer distance (6.53 Å) and (b) interlayer distance ($d = 6.65$ Å).

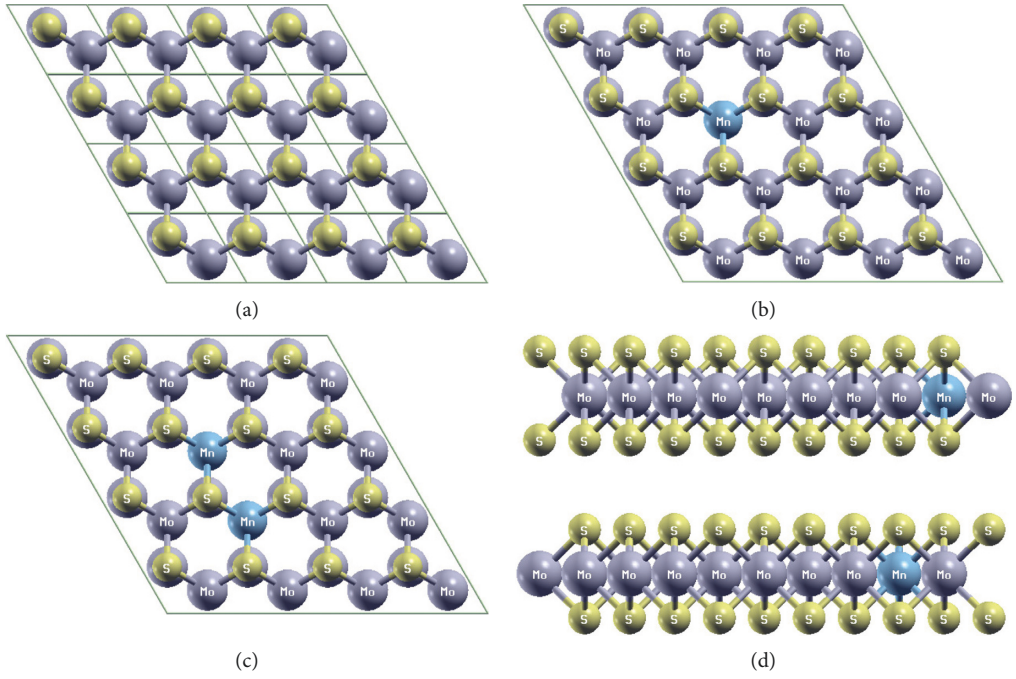

Figure 2: Optimized input structures of $4 \times 4 \times 1$ BL MoS_2: (a) top view for pure BL MoS_2; (b) top view for one Mn-doped BL MoS_2; (c) top view for two Mn-doped BL MoS_2; (d) side view for two Mn-doped BL MoS_2

Table 2: The calculated magnetic energy ($\Delta E = E_{FM} - E_{AF}$) and magnetic moment ($\mu_m$) for ML MoS_2-doped Mn.

Supercell	Distance (d)	Impurity (%)	ΔE (eV)	μ_m
$3 \times 3 \times 1$	Single	11.11	—	1.00
>>	N	22.22	−0.18444	2.32
>>	NN	22.22	−0.212240	2.000
>>	NNN	22.22	−0.132042	2.74
$4 \times 4 \times 1$	Single	6.250	–	1.00
>>	N	12.50	−0.21007	2.07
>>	NN	12.50	−0.177582	2.00
>>	NNN	12.50	−0.0849	2.00
$5 \times 5 \times 1$	N	8.00	−0.1636	2.46

bond angle (Mn-S-Mn) is calculated as 93° which is closer to 90° and ensures that FM super exchange is primarily response for magnetic interaction in nearest neighbor dopants, in other words, Mn $3d$ orbital electrons interact antiferromagnetically with one of sulfur (S) $3p$ electrons then this state further interacts with other Mn $3d$ electrons; in this way, the two Mn atoms communicate ferromagnetically indirectly with aid of sulfur $3p$ state. We now turn to investigate the role of interlayer interaction in BL MoS_2, and we make magnetic energy, ΔE, comparison between pair of Mn-doped MoS_2 ML with BL MoS_2 using a $5 \times 5 \times 1$, $4 \times 4 \times 1$, and $3 \times 3 \times 1$ supercells, and the results are listed

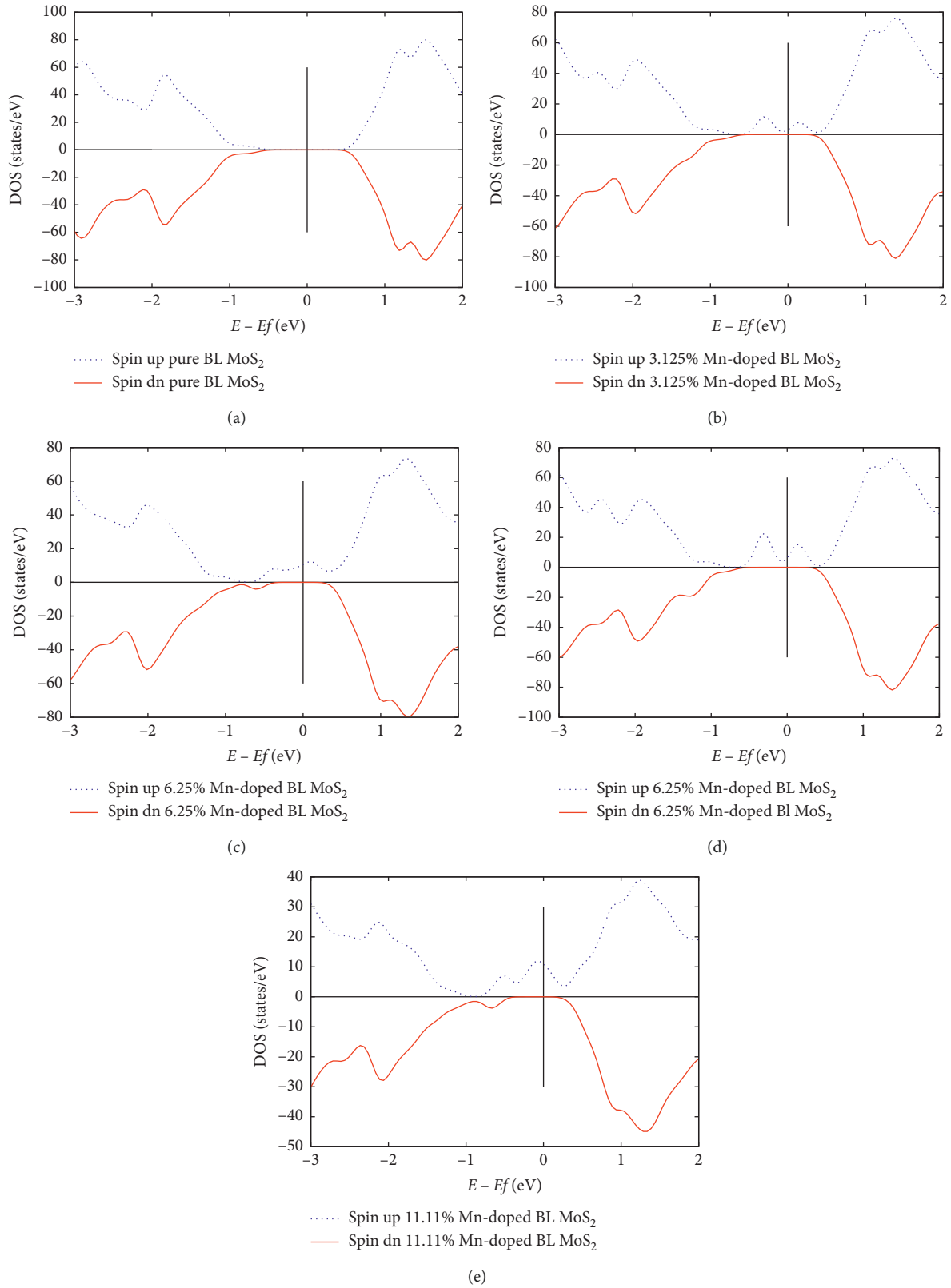

FIGURE 3: Total density of states (DOS) for $4 \times 4 \times 1$ BL MoS_2 (a) pure, (b) one Mn doped $4 \times 4 \times 1$ MoS_2 BL, (c) two Mn doped (in the same layer) $4 \times 4 \times 1$ BL MoS_2, (d) two Mn (one in the upper layer and the other in the lower layer) doped $4 \times 4 \times 1$ BL MoS_2, and (e) two Mn (in the same layer) doped $3 \times 3 \times 1$ BL MoS_2. The blue and red lines represent the spin-up and spin-down components, respectively; the vertical thin line indicates the Fermi level.

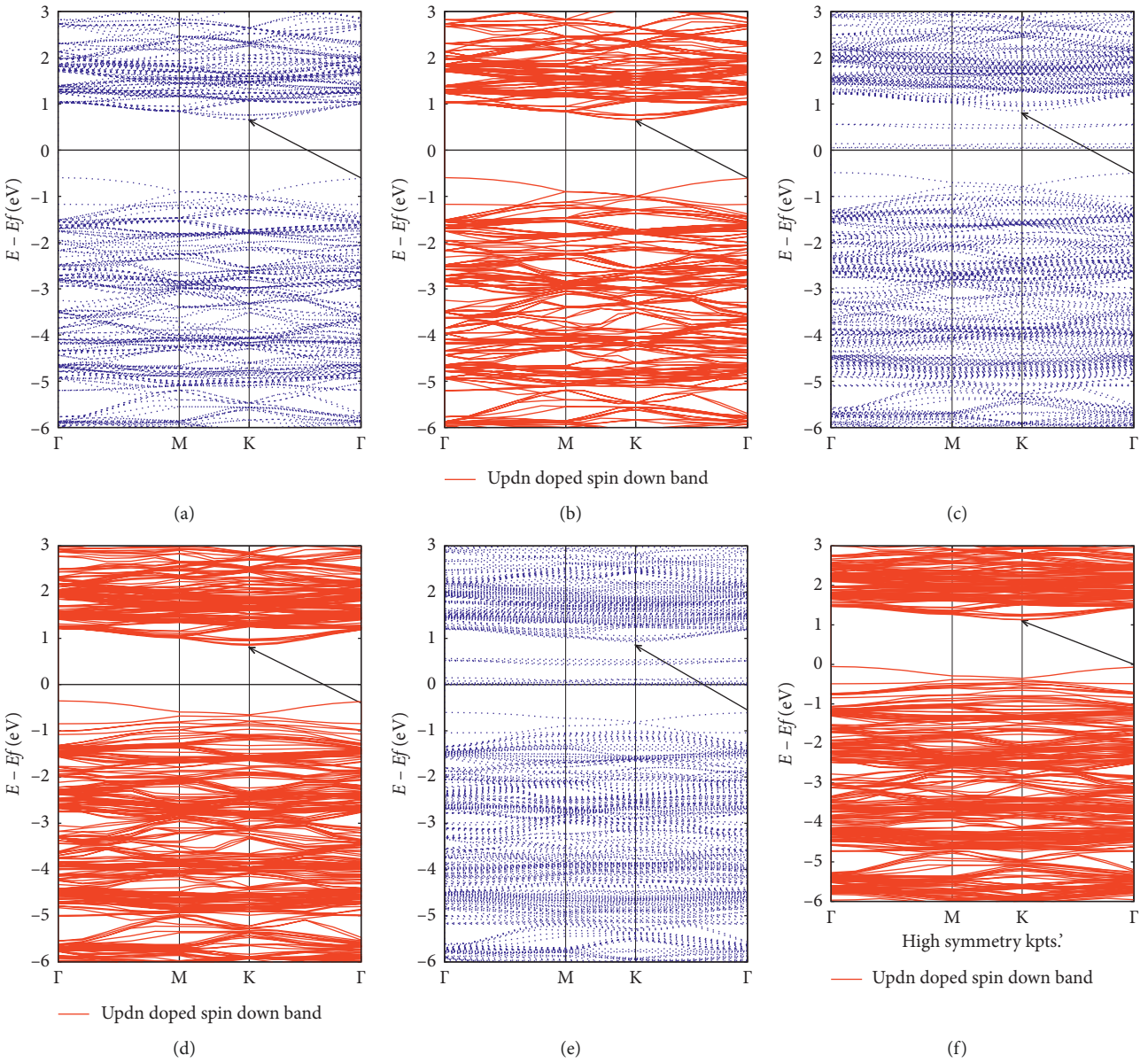

FIGURE 4: Band structures of $4 \times 4 \times 1$ bilayer MoS_2: (a) and (b) pure MoS_2; (c) and (d) one Mn-doped in the upper layer of MoS_2 bilayer; (e) and (f) two Mn-doped MoS_2 bilayer(in different layers). The blue and red lines represent the spin-up and spin-down components, respectively. The zero energy represents the Fermi level.

in Tables 3 and 4, respectively. For instance, the calculated (ΔE) are −0.1636, −0.2107, and −0.1844 eV for a pair of Mn doping in the first nearest neighbor (N) configurations in $5 \times 5 \times 1$, $4 \times 4 \times 1$, and $3 \times 3 \times 1$ in ML supercell, respectively, whereas −0.1666, −0.2137, and −0.192 eV for a pair of Mn doped in nearest neighbor configuration (N) in $5 \times 5 \times 1, 4 \times 4 \times 1$, and $3 \times 3 \times 1$ BL MoS_2 supercells, respectively. The result show that ferromagnetism is more stable in Mn-doped BL MoS_2 than Mn-doped BL MoS_2. The origin of discrepancy between BL and ML MoS_2 in magnetic energy, ΔE, seems to be from interlayer interaction in BL MoS_2. Therefore, we report that interlayer interaction in Mn-doped BL MoS_2 system can affect its magnetic interaction, and similar finding was recently reported in iron-doped BL MoS_2 [14].

3.4. Ferromagnetic Transition Temperature (T_c). By mapping Heisenberg Hamiltonian together with mean field approximation, the Curie temperature (T_c) below which the system develops a long-range ferromagnetic ordering can be found as follows [27]:

$$\frac{3}{2} k_B T_c = -\frac{\Delta E}{N}, \tag{3}$$

where $\Delta E = E_{FM} - E_{AF}$ is the magnetic energy obtained from the first principle spin polarized DFT calculation and N is the number of dopants in supercell. Using the value ΔE for first nearest neighbor impurity configurations (N) in Table 3 and $N = 2$, we have calculated ferromagnetic transition (T_c) for Mn-doped BL MoS_2. However, it is well known that the magnetic ordering in the doped system is strongly

Table 3: The calculated magnetic energy ($\Delta E = E_{FM} - E_{AF}$) and magnetic moment ($\mu_m$) for BL MoS_2-doped Mn.

Supercell	Distance (d)	Impurity (%)	ΔE (eV)	μ_m
$3\times3\times1$	Single	5.55		1.00
>>	N	11.11	−0.192	2.13
>>	NN	11.11	−0.232	2.000
>>	NNN	11.11	−0.13046	1.83
>>	updn(do)	11.11	−0.0085	2.00
>>	updn(d1)	11.11	−0.0033	2.000
$4\times4\times1$	Single	3.125		1.02
>>	N	6.25	−0.2137	2.03
>>	NN	6.25	−0.169	2.00
>>	NNN	6.25	−0.08217	2.06
>>	updn(do)	6.25	−0.006	2.00
>>	updn(d1)	6.25	−0.0025	2.00
$5\times5\times1$	N	4.00	−0.166	2.46

Table 4: The calculated ferromagnetic transition temperature (T_c) for Mn-doped bilayer MoS_2.

System	Impurity (%)	ΔE	T_c^{MFA} (K)	T_c^{corr}
Bilayer MoS_2-doped Mn	4.000	−0.166	641	324
>>	6.25	−0.214	827	418
>>	11.11	−0.192	742	381

influenced by percolation, and thus mean-field approximation cannot capture this behavior and tends to systematically overestimate T_c in these systems [13]. To overcome this, we make use of some empirical relation which connects the mean field value critical temperature T_c^{MFA} with corrected critical temperature (T_c^{corr}) as $T_c^{corr} = (0.506)T_c^{MFA}$ [28], where T_c^{corr} is the exact (corrected) critical temperature for 2D hexagonal lattice calculated using Ising model and T_c^{MFA} is the predicted critical temperature using mean field theory. The calculated result is presented in Table 4. As shown in Table 4, T_c in Mn-doped BL MoS_2 is found to be above the room temperature (RT), and a nonmonotonic behavior of T_c is observed; T_c increases with Mn concentrations in a range of dilute limit (0 to 6.25%) and then decreases with further increasing Mn concentration above this value (6.25 to 11.11%), which confirm that, at high concentrations, the system exhibits FM instability due to some sort of direct interaction. Thus, the result indicates that ferromagnetism in this system is tunable by controlling the concentration of magnetic dopants (Mn), and such kind of properties are seen in well-known III-V DMS [10].

4. Conclusion

In conclusion, Mn dopant in BL MoS_2 are energetically favorable to occupy the substitutional lattice site (Mo) under sulfur- (S-) rich regime than Mo. The magnetic interaction between dopants in Mn-doped BL MoS_2 is always ferromagnetic. Moreover, the strength of ferromagnetism decays with atomic distance. Interlayer interaction in Mn-doped BL MoS_2 affects its magnetic properties. Super exchange mechanism is primarily responsible for ferromagnetic interaction between a pair of dopants. The calculated T_c shows that good dilute limit of dopant concentration is 0 − 6.25%, and further increasing dopant concentration results in FM instability. Based on the result, it is suggested that Mn-doped BL MoS_2 are promising candidates for 2D dilute magnetic superconductors for high-temperature spintronics applications.

Data Availability

The data used to support the findings of this study are available from the corresponding author upon request.

Conflicts of Interest

The authors declare that there are no conflicts of interest.

Acknowledgments

The authors acknowledge financial support from the Center for Science and Technology of the Non-Aligned and Other Developing Countries (NAM S & T Center), Supercomputer Education and Research Center (SERC) at Indian Institute of Sciences (IISc) for providing the computational facilities, and Arba Minch University, Arba Minch, Ethiopia.

References

[1] V. Parashar, C. P. Durand, B. Hao et al., "Switching behaviors of graphene-boron nitride nanotube heterojunctions," *Scientific Reports*, vol. 5, no. 1, Article ID 12238, 2015.

[2] T. Cheiwchanchamnangij and W. R. L. Lambrecht, "Quasiparticle band structure calculation of monolayer, bilayer, and bulk MoS_2," *Physical Review B*, vol. 85, no. 20, Article ID 205302, 2012.

[3] K. S. Novoselov, A. K. Geim, S. V. Morozov et al., "Electric field effect in atomically thin carbon films," *Science*, vol. 306, no. 5696, pp. 666–669, 2004.

[4] C. J. Gil, A. Pham, A. Yu, and S. Li, "An ab initio study of transition metals doped with WSe_2 for long-range room temperature ferromagnetism in two-dimensional transition metal dichalcogenide," *Physics: Condensed Matter*, vol. 26, no. 30, Article ID 306004, 2014.

[5] Q. H. Wang, K. Kalantar-Zadeh, A. Kis, J. N. Coleman, and M. S. Strano, "Electronics and optoelectronics of two-dimensional transition metal dichalcogenides," *Nature Nanotechnology*, vol. 7, no. 11, pp. 699–712, 2012.

[6] S. W. Han, H. Kwon, S. K. Kim et al., "Band-gap transition induced by interlayer van der Waals interaction in MoS_2," *Physical Review B*, vol. 84, no. 4, Article ID 045409, 2011.

[7] Y. C. Cheng, Z. Y. Zhu, W. B. Mi, Z. B. Guo, and U. Schwingenschlögl, "Prediction of two-dimensional diluted magnetic semiconductors: Doped monolayer MoS_2 systems," *Physical Review B*, vol. 87, no. 10, Article ID 100401, 2013.

[8] J. He, K. Hummer, and C. Franchini, "Stacking effects on the electronic and optical properties of bilayer transition metal dichalcogenidesMoS_2, $MoSe_2$, WS_2, and WSe_2," *Physical Review B*, vol. 89, no. 7, Article ID 075409, 2014.

[9] M. Yahyaoui, K. Boujdaria, M. Cubukcu, C. Testelin, and C. Gourdon, "The influence of phosphorus content on magnetic anisotropy in ferromagnetic (Ga, Mn) (As, P)/GaAs thin films," *Journal of Physics: Condensed Matter*, vol. 25, no. 34, Article ID 346001, 2013.

[10] M. Shahjahan, I. M. Razzakul, and M. M. Rahman, "First-principles calculation of stable magnetic state and Curie

temperature in transition metal doped III-V semiconductors," *Computational Condensed Matter*, vol. 9, pp. 67–71, 2016.

[11] J. Deng, C. Pei, W. Wang et al., "The structural and magnetic properties of Fe/(Ga, Mn)As heterostructures," *Journal of Semiconductors*, vol. 34, no. 8, Article ID 083003, 2013.

[12] R. Mishra, Z. Wu, S. J. Pennycook, S. T. Pantelides, and J.-C. Idrobo, "Long-range ferromagnetic ordering in manganese-doped two-dimensional dichalcogenides," *Physical Review B*, vol. 88, no. 14, Article ID 144409, 2013.

[13] A. Ramasubramaniam and D. Naveh, "Mn-doped monolayer MoS_2: an atomically thin dilute magnetic semiconductor," *Physical Review B*, vol. 87, no. 19, Article ID 195201, 2013.

[14] H. Shu, P. Luo, P. Liang, D. Cao, and X. Chen, "Layer-dependent dopant stability and magnetic exchange coupling of iron-doped MoS2 nanosheets," *ACS Applied Materials & Interfaces*, vol. 7, no. 14, pp. 7534–7541, 2015.

[15] M. Luo, Y. H. Shen, and J. H. Chu, "First-principles study of the magnetism of Ni-doped MoS_2 monolayer," *Japanese Journal of Applied Physics*, vol. 55, no. 9, Article ID 093001, 2016.

[16] Y. Yue, C. Jiang, Y. Han, M. Wang, J. Ren, and Y. Wu, "Magnetic anisotropies of Mn-, Fe-, and Co-doped monolayer MoS2," *Journal of Magnetism and Magnetic Materials*, vol. 496, Article ID 165929, 2020.

[17] S. Mekonnen and P. Singh, "Electronic structure and nearly room-temperature ferromagnetism in V-doped monolayer and bilayer MoS_2," *International Journal of Modern Physics B*, vol. 32, no. 21, Article ID 1850231, 2018.

[18] F. Zhou, K. Kang, T. Maxisch, G. Ceder, and D. Morgan, "The electronic structure and band gap of $LiFePO_4$ and $LiMnPO_4$," *Solid State Communications*, vol. 132, no. 3-4, pp. 181–186, 2004.

[19] S. Grimme, J. Antony, S. Ehrlich, and H. Krieg, "A consistent and accurate ab initio parametrization of density functional dispersion correction (DFT-D) for the 94 elements H-Pu," *The Journal of Chemical Physics*, vol. 132, no. 15, Article ID 154104, 2010.

[20] H. J. Monkhorst and J. D. Pack, "Special points for Brillouin-zone integrations," *Physical Review B*, vol. 13, no. 12, pp. 5188–5192, 1976.

[21] K. Dolui, I. Rungger, C. Das Pemmaraju, and S. Sanvito, "Possible doping strategies for MoS_2 monolayers: anab initiostudy," *Physical Review B*, vol. 88, no. 7, Article ID 075420, 2013.

[22] J. Suh, T.-E. Park, D.-Y. Lin et al., "Doping against the native propensity of MoS_2: degenerate hole doping by cation substitution," *Nano Letters*, vol. 14, no. 12, pp. 6976–6982, 2014.

[23] S. Jimnez Sandoval, D. Yang, R. F. Frindt, and J. C. Irwin, "Structure of single-molecular-layer MoS_2," *Physical Review B*, vol. 43, no. 14, pp. 12053–12056, 1991.

[24] H. Wan, L. Xu, W.-Q. Huang et al., "Band structure engineering of monolayer MoS_2: a charge compensated codoping strategy," *RSC Advances*, vol. 5, no. 11, pp. 7944–7952, 2015.

[25] R. Wang, X. Zhou, X. Xu, J. Hu, and J. Pan, "The indirect–direct band gap tuning in armchair MoS_2 nanoribbon by edge passivation," *Journal of Physics D: Applied Physics*, vol. 50, no. 9, Article ID 095102, 2017.

[26] K. Sato, P. H. Dederics, and H. Katayama-Yoshida, "Curie temperatures of III-V diluted magnetic semiconductors calculated from first principles," *Europhysics Letters (EPL)*, vol. 61, no. 3, pp. 403–408, 2003.

[27] Y. Wang, S. Li, and J. Yia, "Electronic and magnetic properties of Co doped MoS_2 monolayer," *Scientific Reports*, vol. 6, no. 1, Article ID 24153, 2016.

[28] N.W. Aschcroft and N. David Memer, *Solid State Physics*, Harcourt College Publisher, New York, NY, USA, 1976.